Heliyon 9 (2023) e21711

Contents lists available at ScienceDirect

Heliyon

journal homepage: www.cell.com/heliyon

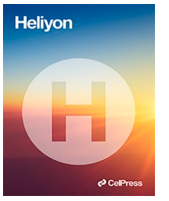

Network pharmacology and in vitro experimental verification to reveal the mechanism of Astragaloside IV against kidney ischemia-reperfusion injury

Yan Guo [a,c,1], Jinfu Wang [b,1], Yanjie Hua [b], Mengya Jiang [a,c], Wanyue Xu [a,c], Yanpeng Shi [d], Jiehong Yang [b], Haitong Wan [b,**], Ruchun Yang [a,c,*]

[a] Hangzhou TCM Hospital Affiliated to Zhejiang Chinese Medical University, Hangzhou, Zhejiang, 310053, China
[b] Zhejiang Chinese Medical University, Hangzhou, Zhejiang, 310053, China
[c] Key Laboratory of Kidney Disease Prevention and Control Technology, Zhejiang Province, 310053, China
[d] Linping Hospital of Integrated Traditional Chinese and Western Medicine, Hangzhou, Zhejiang, 310053, China

ARTICLE INFO

Keywords:
Astragaloside IV
Kidney ischemia-reperfusion injury
Ferroptosis
Network pharmacology
Molecular docking
Molecular dynamics simulations

ABSTRACT

Ischemic acute kidney injury (AKI) is a prevalent disorder among hospitalized patients worldwide. Astragaloside IV (AS-IV) has been shown to protect against ischemic AKI. However, the specific effects and mechanisms of AS-IV on alleviating kidney ischemia-reperfusion (I/R) injury remain unclear. The objective of this research was to elucidate the regulatory targets and mechanisms through which AS-IV protects kidney I/R injury. A combination of network pharmacology, molecular docking, molecular dynamics (MD) simulation, pharmacodynamic study and Western blot were employed to explore the underlying mechanisms. Network pharmacology revealed that ferroptosis was a potential mechanism of AS-IV against kidney I/R injury. Molecular docking and MD simulations demonstrated strong binding affinity between the GPX4/SLC7A11 and AS-IV. The experimental verification demonstrated that AS-IV improved cell proliferation, decreased the level of ROS and Fe^{2+}, and increased the expressions of GPX4 and SLC7A11 as same as Ferrostatin-1 in OGD/R-injured HUVECs. In conclusion, AS-IV had a significant inhibition on ferroptosis in kidney I/R injury, providing a new perspective for drug development on kidney I/R injury. Definitely, further exploration in vivo is necessary to fully understand whether AS-IV alleviates kidney I/R injury through inhibiting endothelial ferroptosis.

1. Introduction

Acute kidney injury (AKI) is a prevalent clinical disorder worldwide among hospitalized patients, which moreover probably progress to the chronic kidney diseases (CKD) and end-stage renal disease [1,2]. AKI caused by kidney ischemia-reperfusion injury (kidney I/R injury) results from the acute limitation of arterial blood flow to the kidneys, followed by reperfusion creating a mismatch

* Corresponding author. Hangzhou TCM Hospital Affiliated to Zhejiang Chinese Medical University, Hangzhou, Zhejiang, 310053, China.
** Corresponding author. Zhejiang Chinese Medical University, Hangzhou, Zhejiang, 310053, China
E-mail addresses: joygy1401@163.com (Y. Guo), wangjinfu@zcmu.edu.cn (J. Wang), huayj22@126.com (Y. Hua), 17775483815@139.com (M. Jiang), xuwanyue73@163.com (W. Xu), syp161210@163.com (Y. Shi), yjhong@zcmu.edu.cn (J. Yang), whtong@126.com (H. Wan), yangruchunhz@163.com (R. Yang).
[1] Yan Guo and Jinfu Wang contributed equally to this work.

https://doi.org/10.1016/j.heliyon.2023.e21711
Received 4 July 2023; Received in revised form 26 October 2023; Accepted 26 October 2023
Available online 31 October 2023

between oxygen and nutrient supply, damages endothelial cells, and leading to continuous renal failure [3,4]. However, there is no effective therapy that can significantly alleviate kidney I/R injury immediately, thus, preventing the development of renal disease. Fortunately, compounds originating from Chinese herbal medicines have emerged as a promising option for treating kidney I/R injury.

Astragaloside IV (AS-IV) is a major bioactive compound of Astragalus membranaceus, and has been linked to numerous of pharmacological functions such as antioxidative properties, endothelial function protection, and promotion of vascular regeneration [5–7]. Previous studies have demonstrated that AS-IV could mitigate renal I/R injury [8]. However, the regulatory targets and mechanisms for AS-IV ameliorating kidney I/R injury requires further elucidation.

Network pharmacology is an emerging research field for investigating the mechanisms among drugs with diseases [9]. Currently, it is a growing trend to investigate the mechanisms of traditional Chinese medicine (TCM) with characteristics of multi-component, multi-channel and multi-target synergy using network pharmacology [10–12]. The combination of network pharmacology and experimental verification has been recognized as a powerful approach to fully elucidate the mechanisms and impacts of TCM, surpassing the limitations of the single experimental studies [13]. Therefore, in this study, the network pharmacology analysis and experimental verification were used to identify the possible targets and mechanism of AS-IV alleviating kidney I/R injury.

2. Results and discussion

2.1. Target fishing

2.1.1. Identification of AS-IV targets

The molecular structure of AS-IV is illustrated in Fig. 1A. The Swiss Target Prediction database was used to identify 100 predicted targets for AS-IV. Afterwards, A total of 30 targets with probability greater than 0 can be obtained, and an additional 20 distinct genes for AS-IV were provided by the relevant literatures [14–20]. Ultimately, 50 genes were identified for additional analysis.

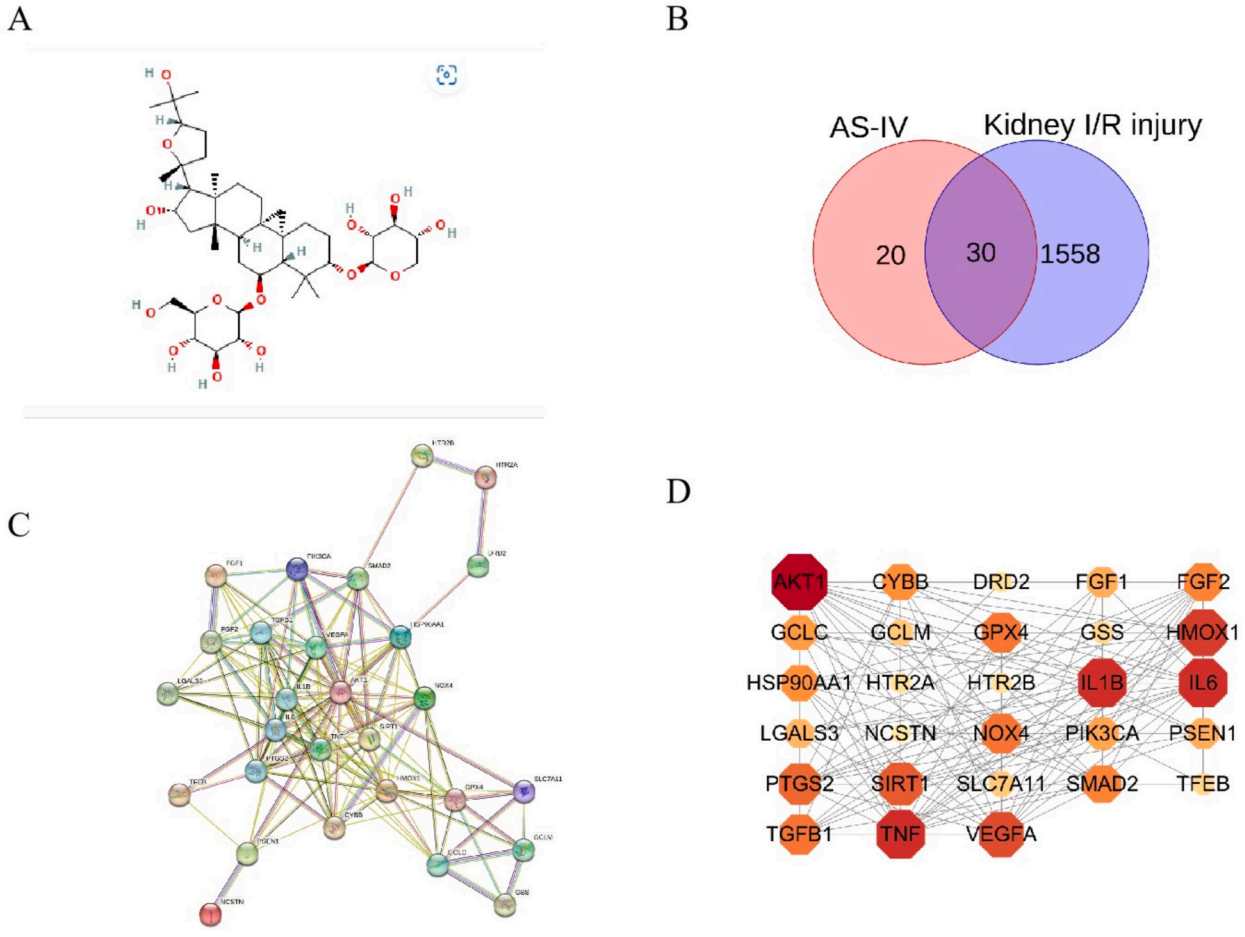

Fig. 1. Identification of targets. (A) The chemical structure of AS-IV, (B) A Venn diagram illustrating shared targets between AS-IV and kidney I/R injury, (C, D) Network visualization of the genes correlated with AS-IV alleviating kidney I/R injury.

2.1.2. Prediction of targets for AS-IV treatment in kidney I/R injury

After eliminating duplicate targets and unify names, a total of 1588 targets correlated with kidney I/R injury were collected in the GeneCards and OMIM databases. And a total of 30 shared targets were found by analyzing the Venn diagram illustrating the overlap between kidney I/R injury and AS-IV targets (Fig. 1B). These findings suggested that 60 % of AS-IV targets were correlated with kidney I/R injury.

2.1.3. Constructing a protein-protein interaction (PPI) network

The PPI network of 30 targets was visualized using the String database (Fig. 1C). And the analysis was performed using Cytoscape 3.9.1 software to identify the key indicators associated with kidney I/R injury. The significance of these indicators were represented by the color and size of the nodes, with darker and bigger nodes indicating greater importance (Fig. 1D).

2.2. GO enrichment analysis

For investigating the potential regulation of signaling pathways correlate with kidney I/R injury by AS-IV, Gene Ontology (GO) enrichment analysis were conducted using the 30 targets shared by AS-IV and kidney I/R injury. A total of 815 items were identified in three categories: 749 biological processes (BP), 25 molecular functions (MF), and 41 cellular components (CC). Three bubble charts visualizing the top 20 enriched terms for each category (Fig. 2A–C), and a column chart displaying the 10 terms with the highest gene counts in each category (Fig. 2D). The top five enriched BP terms included the positive regulation of protein phosphorylation, phosphorylation, protein kinase activity, protein serine/threonine kinase activity, and kinase activity. The highly enriched MF terms included growth factor receptor binding, receptor ligand activity, signaling receptor activator activity, signaling receptor regulator activity, and cytokine activity. The CC terms included neuronal cell body, membrane raft, membrane microdomin, cell body, and presynaptic membrane.

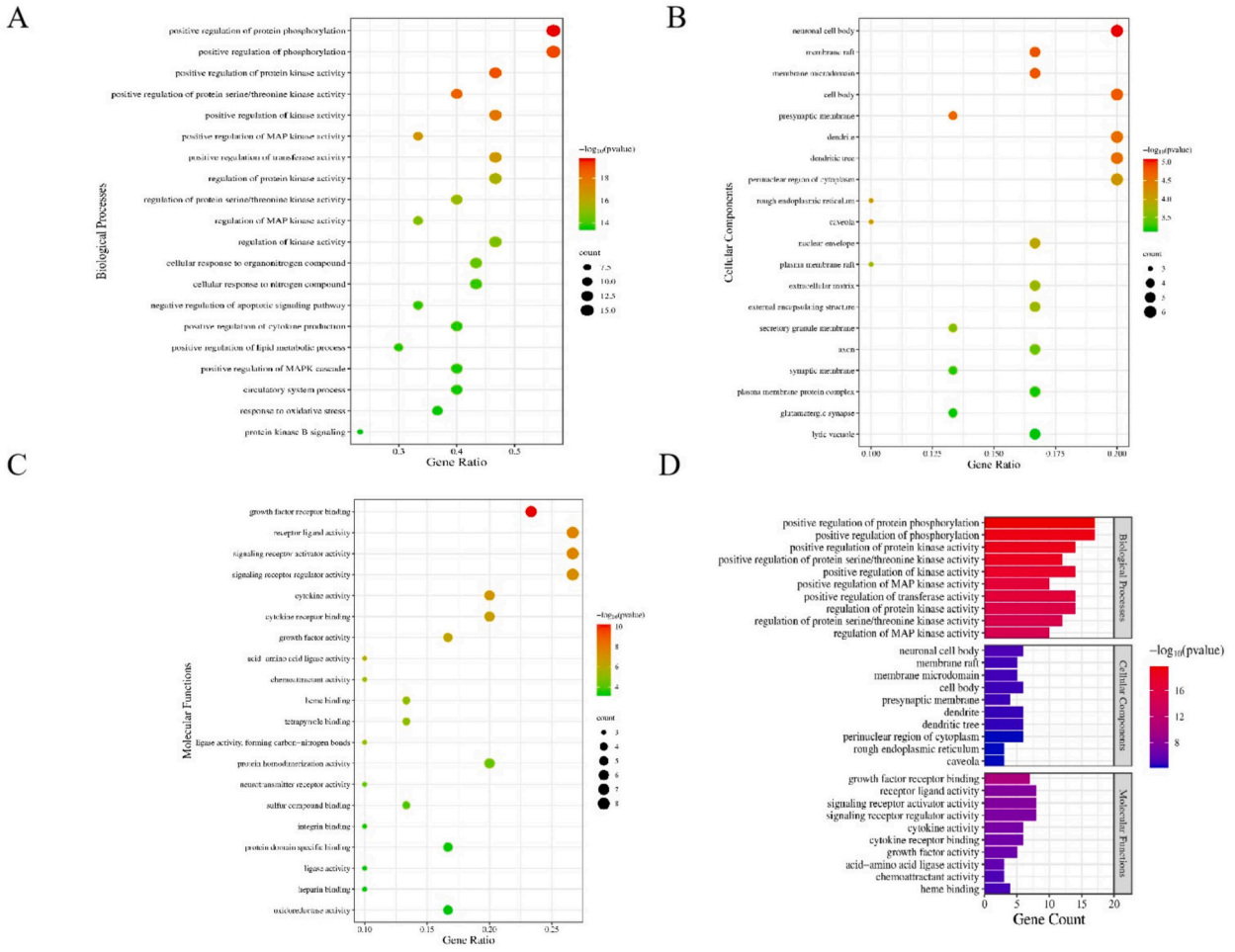

Fig. 2. Display of GO enrichment analysis results. (A) Bubble chart of GO terms in the BP category. (B) Bubble chart of GO terms in the CC category. (C) Bubble chart of GO terms in the MF category. (D) Top 10 GO terms in the BP, CC and MF categories of GO enrichment analysis.

2.3. KEGG analysis

KEGG analysis was conducted on the 30 targets of AS-IV and kidney I/R injury. A total of 105 pathways were identified with a significance level of adjusted $P < 0.01$. And Fig. 3A displays the extent of enrichment for the top 20 KEGG pathways, which were further used to create a compound-target-pathway-disease network, as shown in Fig. 3B and Table 1. By constructing the network, the numerous targets and pathways involved in AS-IV alleviating kidney I/R injury were revealed. A bioinformatics platform was used to construct a Sankey diagram (Fig. 3C) to illustrate the connections between target genes and enriched pathways. Subsequent examination showed that AS-IV played a significant role in regulating the AGE-RACE signaling pathway, ferroptosis, cell senescence and others. Thus, it is speculated that AS-IV may reduce kidney I/R injury by regulating the ferroptosis pathway. Furthermore, the ferroptosis pathway was visualized using a bioinformatics platform, revealing that Glutathione Peroxidase 4 (GPX4) and Solute Carrier Family 7 Member 11(SLC7A11) were key targets related to ferroptosis (Fig. 3D).

2.4. Molecular docking

Based on the KEGG analysis, GPX4 and SLC7A11 were selected as potential molecular targets for AS-IV. Molecular docking was carried out using AutoDock Tools 1.5.7 software, and the results indicated low binding energy of AS-IV when docked with GPX4 (−4.74 kcal/mol) and SLC7A11 (−3.37 kcal/mol). The binding sites of AS-IV with GPX4 or SLC7A11 were further analyzed, revealing three hydrogen bonding with residues ASN-124, LYS-126, LYS-117 of GPX4 (Fig. 4A), and three hydrogen bonding with residues THR-485, LEU-351, TRP-128 of SLC7A11 (Fig. 4B). These results suggested that GPX4 and SLC7A11 bind with AS-IV steadily [21].

2.5. Molecular dynamics (MD) simulations provide evidence for the stability of protein-ligand complexes

MD simulation was performed to analyze the structural characteristics, trajectory, binding potential, molecules motion, and conformational alterations of GPX4 and SLC7A11 proteins with AS-IV based on the molecular docking results (Fig. 5A1-B4). Short-

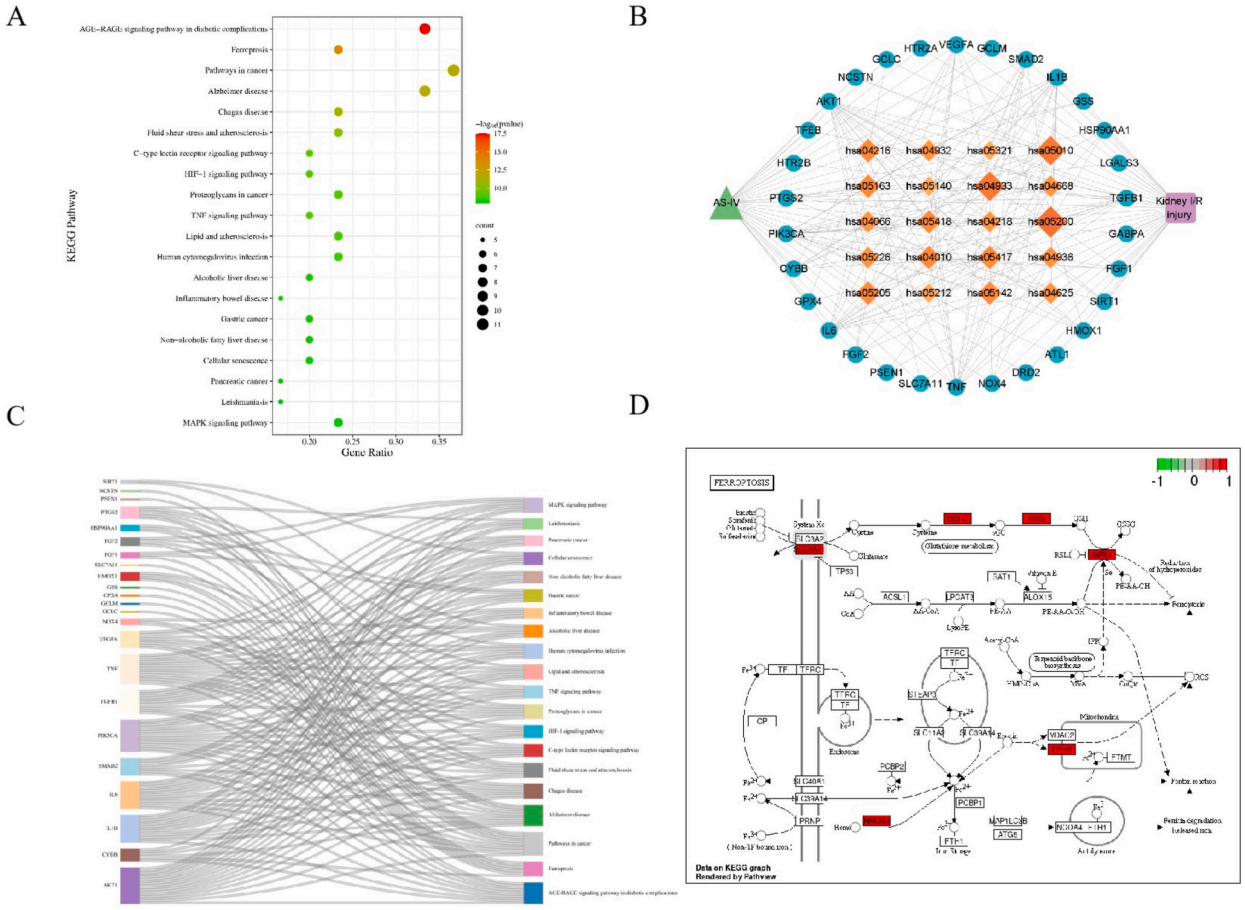

Fig. 3. Display of KEGG enrichment analysis results. (A) The bubble chart of the top 20 pathways. (B) The diagram of compound-target-pathway-disease network. (C) The sankey diagram of the top 20 pathways and therapeutic targets. (D) The map of ferroptosis pathway.

Table 1
KEGG pathway analysis of critical genes.

ID	Description	Count	Gene	Pvalue
hsa04933	AGE-RAGE signaling pathway in diabetic complications	10	AKT1,CYBB,IL1B,IL6,SMAD2,PIK3CA,TGFB1,TNF,VEGFA,NOX4	2.85378E-18
hsa04216	Ferroptosis	7	CYBB, GCLC,GCLM,GPX4,GSS,HMOX1,SLC7A11	9.89034E-15
hsa05200	Pathways in cancer	11	AKT1,FGF1,FGF2,HMOX1,HSP90AA1,IL6,SMAD2,PIK3CA,PTGS2, TGFB1,VEGFA	1.82147E-12
hsa05010	Alzheimer disease	10	AKT1,CYBB,IL1B,IL6,PIK3CA,PSEN1,PTGS2,TNF,NCSTN,NOX4	2.36897E-12
hsa05142	Chagas disease	7	AKT1,IL1B,IL6,SMAD2,PIK3CA,TGFB1,TNF	7.79968E-12
hsa05418	Fluid shear stress and atherosclerosis	7	AKT1,HMOX1,HSP90AA1,IL1B,PIK3CA,TNF,VEGFA	7.02993E-11
hsa04625	C-type lectin receptor signaling pathway	6	AKT1,IL1B,IL6,PIK3CA,PTGS2,TNF	8.0303E-10
hsa04066	HIF-1 signaling pathway	6	AKT1,CYBB, HMOX1,IL6,PIK3CA,VEGFA	1.06803E-09
hsa05205	Proteoglycans in cancer	7	AKT1,FGF2,SMAD2,PIK3CA,TGFB1,TNF,VEGFA	1.07309E-09
hsa04668	TNF signaling pathway	6	AKT1,IL1B,IL6,PIK3CA,PTGS2,TNF	1.25921E-09
hsa05417	Lipid and atherosclerosis	7	AKT1,CYBB,HSP90AA1,IL1B,IL6,PIK3CA,TNF	1.49497E-09
hsa05163	Human cytomegalovirus infection	7	AKT1,IL1B,IL6,PIK3CA,PTGS2,TNF,VEGFA	2.05048E-09
hsa04936	Alcoholic liver disease	6	AKT1,IL1B,IL6,TNF,SIRT1,NOX4	5.27571E-09
hsa05321	Inflammatory bowel disease	5	IL1B,IL6,SMAD2,TGFB1,TNF	5.41243E-09
hsa05226	Gastric cancer	6	AKT1,FGF1,FGF2,SMAD2,PIK3CA,TGFB1	7.04373E-09
hsa04932	Non-alcoholic fatty liver disease	6	AKT1,IL1B,IL6,PIK3CA,TGFB1,TNF	8.92542E-09
hsa04218	Cellular senescence	6	AKT1,IL6,SMAD2,PIK3CA,TGFB1,SIRT1	9.2761E-09
hsa05212	Pancreatic cancer	5	AKT1,SMAD2,PIK3CA,TGFB1,VEGFA	1.20143E-08
hsa05140	Leishmaniasis	5	CYBB,IL1B,PTGS2,TGFB1,TNF	1.28397E-08
hsa04010	MAPK signaling pathway	7	AKT1,FGF1,FGF2,IL1B,TGFB1,TNF,VEGFA	1.30197E-08

range Coulombic interaction energy, short-range Lennard-Jones energy, Root Mean Square Deviation (RMSD), Radius of Gyration (RG), Surface Area (SASA) were analyzed [22]. RMSD is a reliable indicator of the conformational stability of protein-ligand complexes, and the degree of deviation of atomic positions from the starting position. A smaller fluctuation of RMSD value indicates a greater the stability of the protein-ligand complex. The RMSD of the GPX4-AS-IV complex exhibited fluctuations initially but stabilized after 37.5 nm. The RMSD of the SLC7A11-AS-IV complex displayed significant fluctuations initially and eventually stabilized. The conformation of the protein is basically consistent with that of the complex, indicating that AS-IV remained stable after binding to the protein and does not affect its stability. The RG and SASA were observed to study the structural compactness and solvent accessibility of the two complexes. The rotation radius of the GPX4-AS-IV complex remains stable throughout the entire operation process, ranging from 1.6 to 1.7 nm. The rotation radius of the SLC7A11-AS-IV complex showed significant changes in the early stage and stabilized after 40000 ps. The SASA value of GPX4-AS-IV complex ranged between 100 and 120 nm^2, and the SASA value of SLC7A11-AS-IV complex ranged between 405 and 450 nm^2. Short-range Coulombic interaction energy and Jay Jones interaction energy were found to affect the conformation, stability, and affinity of the complex. Our results showed that low interaction energy was required for AS-IV binding with GPX4 and SLC7A11 proteins. Overall, the results of RG, SASA, and protein ligand interaction energy support the numerical fluctuation of RMSD, and the MD simulation strongly confirms the effectiveness of AS-IV docking with GPX4 and SLC7A11 proteins.

2.6. Results of experimental verification

The network pharmacology analysis declared that the ferroptosis pathway may play a crucial role in the process of kidney I/R injury. And, studies have shown that endothelium is a key target for ischemic renal injury [23]. So, human umbilical vein endothelial cells (HUVECs) were used for conducting experiments. First, the results showed that AS-IV (2.5, 1 μM) significantly increased the proliferation of OGD/R-injured HUVECs as same as the Ferrostatin-1(Fer-1, a ferroptosis inhibitor, 5 μM) treatments (Fig. 6A–B), which indicted that AS-IV can protect HUVECs against OGD/R-injury.

Ferroptosis is a novel cell death that primarily arises from iron-dependent lipid peroxidation, and contributes to the formation of

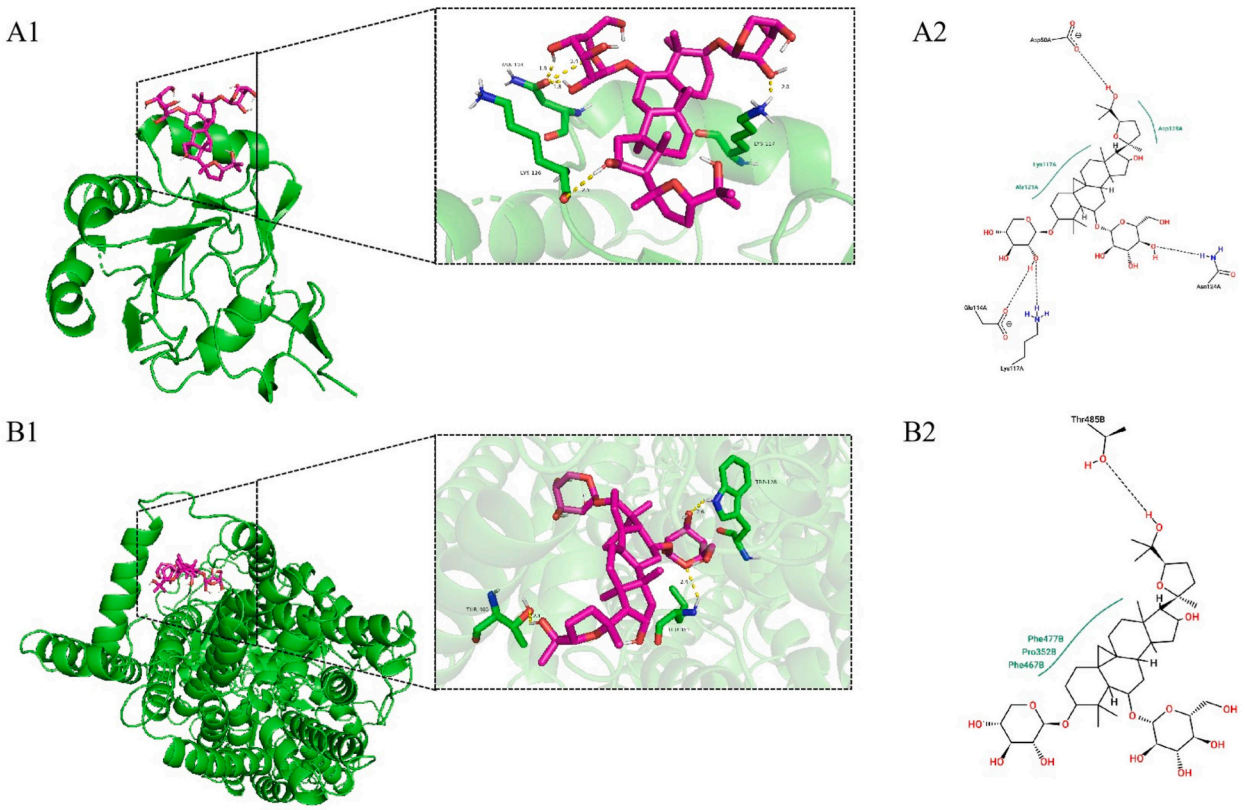

Fig. 4. Docking models of important targets and AS-IV. (A1)GPX4-AS-IV. (B1)SLC7A11-AS-IV. (A2, B2) Two dimensional bond patterns.

ROS [24]. Notably, the accumulation of ROS and intracellular Fe^{2+} are hallmarks of ferroptosis [25], as evidenced by the increase the level of ROS and Fe^{2+} in OGD/R-injured HUVECs. Nonetheless, AS-IV and Fer-1 treatments significantly decreased the level of ROS and Fe^{2+} in OGD/R-injured HUVECs(Fig. 6C–F).

Emerging research has demonstrated that ferroptosis can be provoked by the down-regulation of system Xc (containing SLC7A11 and SLC3A2) activity and the inhibition of GPX4 [26–31]. SLC7A11 serves as the primary active subunit in retrotransport proteins and plays a role in modulating the intracellular equilibrium of GSH [32]. GPX4 acts as a crucial regulator of ferroptosis by converting reduced GSH to oxidized GSH and eliminating intracellular lipid ROS [33]. We likewise discovered that the GPX4 and SLC7A11 expressions were substantially lower in OGD/R group than in the control group. AS-IV treatments significantly increased the GPX4 and SLC7A11 expressions in OGD/R-injured HUVECs, consistent with the Fer-1 effects (Fig. 6G–I).

3. Conclusion

This study indicated AS-IV alleviates ferroptosis in kidney I/R injury, which verified by network pharmacology, molecular docking, MD simulation and experimental verification. AS-IV was shown to decrease the ROS and Fe^{2+} level, and promote the GPX4 and SLC7A11 expressions in OGD/R-injured HUVECs, ultimately restraining ferroptosis in kidney I/R injury. This study proposes a novel target for AS-IV against kidney I/R injury.

Most studies have focused on renal tubular epithelial cells and podocyte dysfunction to study the renal injury. Differently, we are concerned with a relatively novel target of vascular endothelial dysfunction and its relationship with renal injury. Although this study only validated the occurrence of significant endothelial ferroptosis during renal injury through simple in vitro cell experiments. Not unexpectedly, we observed that suppressing the expressions of GPX4 and SLC7A11 aggravated the kidney I/R injury in vivo (as a pre-experiment). Definitely, further exploration in vivo is necessary to fully understand whether AS-IV alleviates kidney I/R injury through inhibiting endothelial ferroptosis.

4. Experimental methods

4.1. Reagents

Astragaloside IV (MDL: MFCD16036240, purity >98 %, HPLC) was purchased from Aladdin (Shanghai, China). The primary antibody against GPX4 (A1933) was purchased from ABclonal technology (Wuhan, China). The primary antibody against SLC7A11

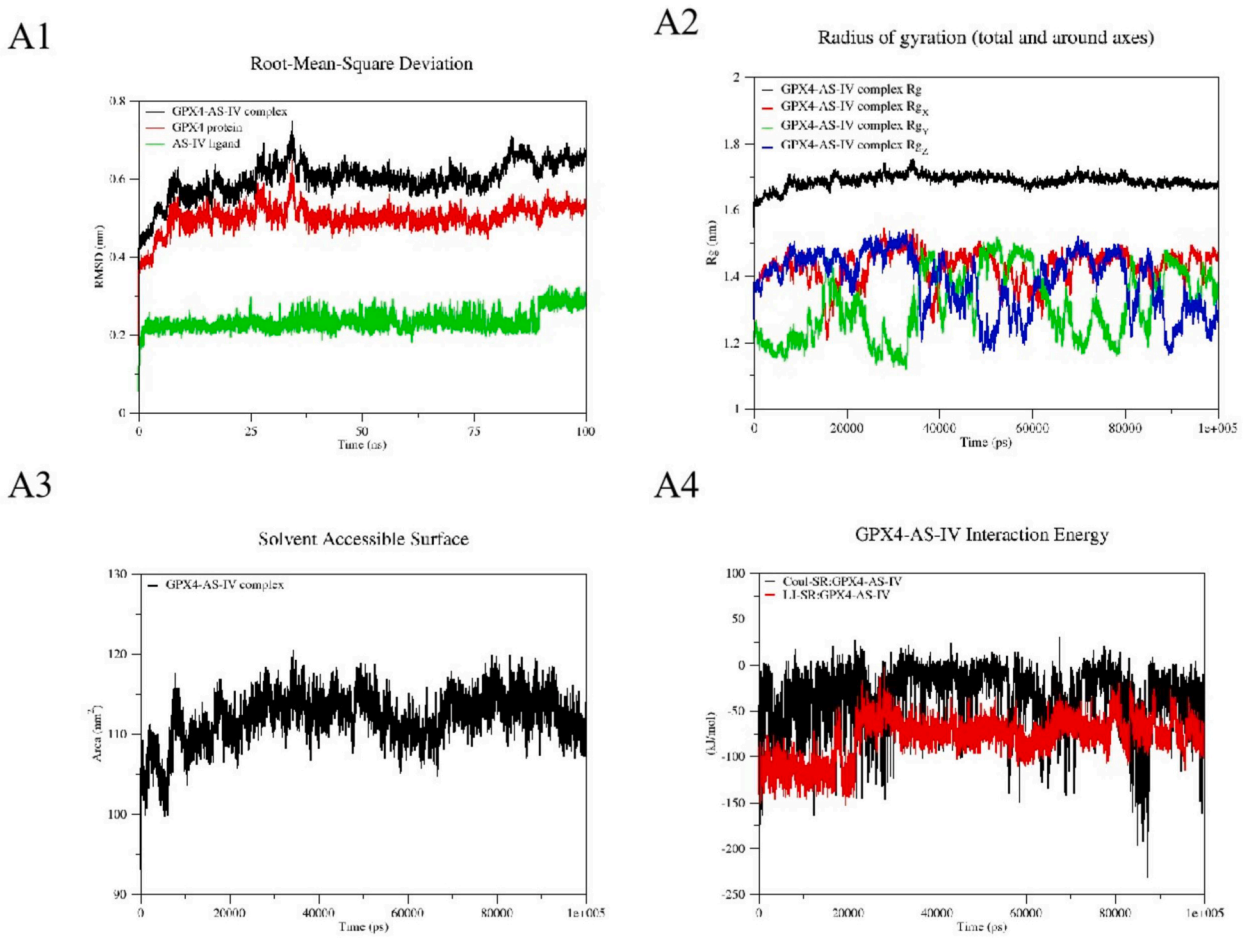

Fig. 5. Molecular dynamics simulation of GPX4 or SLC7A11 with AS-IV. (A1)The RMSD of GPX4-AS-IV. (A2) The RG of GPX4-AS-IV. (A3) The SASA of GPX4-AS-IV. (A4) The interaction energy of GPX4-AS-IV. (B1) The RMSD of SLC7A11-AS-IV. (B2) The RG of SLC7A11-AS-IV. (B3) The SASA of SLC7A11-AS-IV. (B4) The interaction energy of SLC7A11-AS-IV.

(PA1-1683) was purchased from Invitrogen (Carlsbad, California, USA). The primary antibody against GAPDH (60004) was purchased from Proteintech (Wuhan, China).

4.2. Data collection

4.2.1. Identifying therapeutic targets of AS-IV

The potential targets of AS-IV were predicted using the Swiss Target Prediction website (https://www.swisst.argetprediction.ch). In addition, information for other targets was obtained from PubMed.

4.2.2. Construction of kidney I/R injury-related target database

Data for targets correlated with kidney I/R injury were retrieved from two databases: the OMIM database (http://www.omim.org/) and the GeneCards databases (http://www.genecards.org/), using "renal ischemia-reperfusion injury" or "kidney ischemia-reperfusion injury" as the keywords. Finally, the repetitive genes were eliminated.

4.2.3. Intersection between AS-IV and kidney I/R injury-correlated targets

The overlapped targets between the genes correlated with kidney I/R injury and the predicted targets of AS-IV were collected. A Venn diagram was generated using BioLadder (https://www.bioladder.cn/) for visualization.

4.3. Protein-protein interaction (PPI) network construction

An overlapped PPI network was generated using the STRING database (http://string-db.org) focusing on the "*Homo sapiens*". Then,

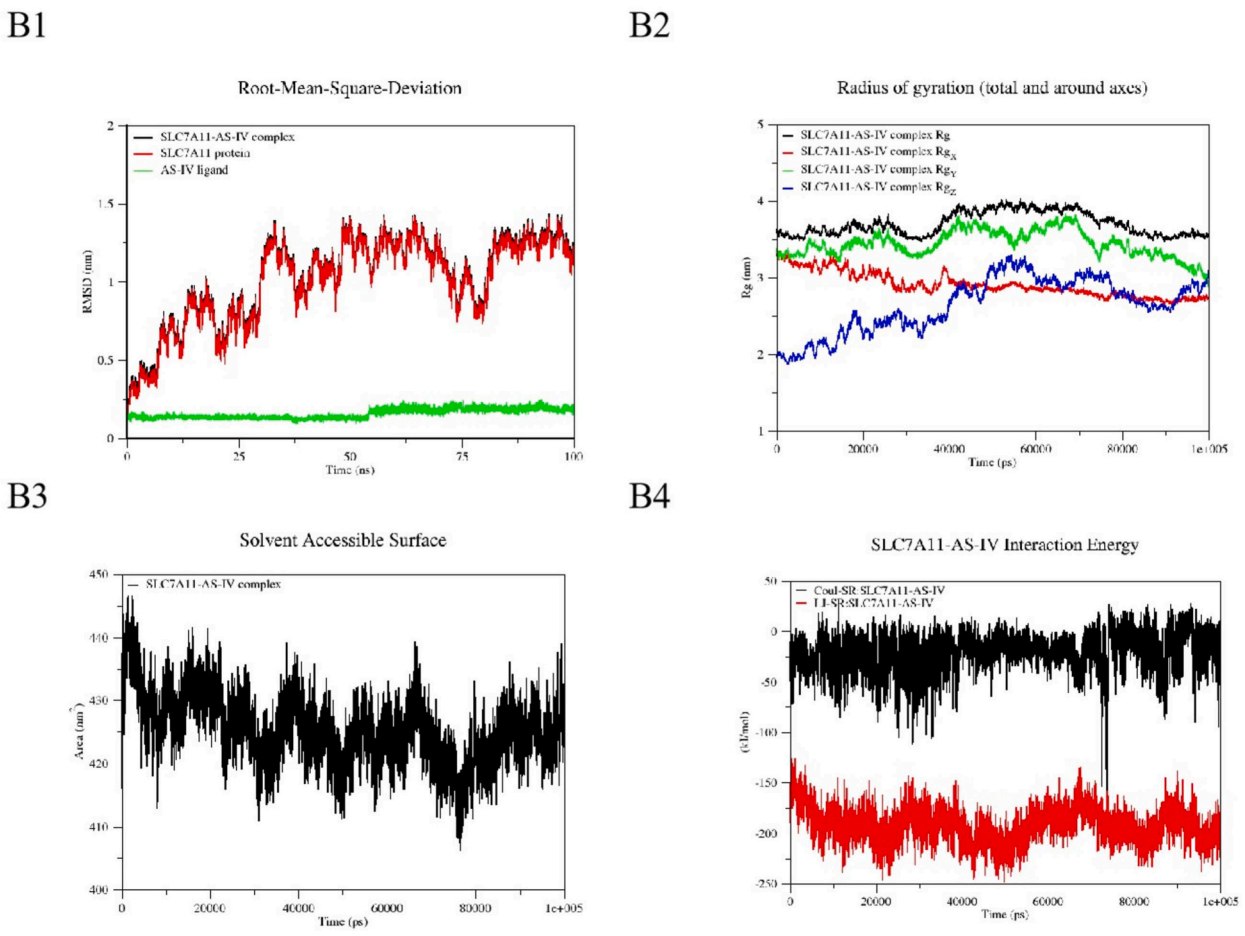

Fig. 5. (*continued*).

the targets without connections were eliminated, and default settings were maintained for other parameters. The software Cytoscape 3.9.1 was employed to create a network featuring possible crucial targets and to systematically analyze the network parameters.

4.4. Gene Ontology (GO) and Kyoto encyclopedia of genes and genomes (KEGG) enrichment analyses

Metascape (www.metascape.org/) was made use of performing GO and KEGG enrichment analyses on intersecting genes, with a cut-off value $P < 0.01$. The results were visualized using bioinformatics platform (https://www.bioinformatics.com.cn/).

4.5. Construction of a compound–target–pathway-disease network

A compound–target–pathway-disease network was constructed and analyzed using Cytoscape 3.9.1 in order to clarify and better understand the intricate links between compound, targets, pathways, and disease.

4.6. Molecular docking verification

The crystal structures of GPX4 and SLC7A11 target proteins (PDB ID: 5H5Q, 7EPZ) were acquired from the Protein Data Bank (https://www.pdbus.org). The PyMOL Molecular Graphics System 2.4.0 program was used to remove water molecules and ligands from the proteins. Then, we used AutoDock Tools 1.5.7 software to add hydrogen atoms, and saved the proteins as pdbqt files. The structure of AS-IV was downloaded from the PubChem database (https://pubchem.ncbi.nlm.nih.gov) and coverted into a 3D structure using the YINFO TECHNOLOGY platform (https://cloud.yinfotek.com/). Atomic charges were added and atom types were assigned to the compound using AutoDock Tools-1.5.7 software. By default, the flexible bonds were set to rotatable and the files were saved in pdbqt format. The AS-IV was used as a small molecule ligand, while the two protein targets served as receptors. Then, AutoDock was utilized to perform molecular docking, and the binding between AS-IV and proteins were visualized using PyMOL2.4.0 and Proteins plus (https://proteins.plus/).

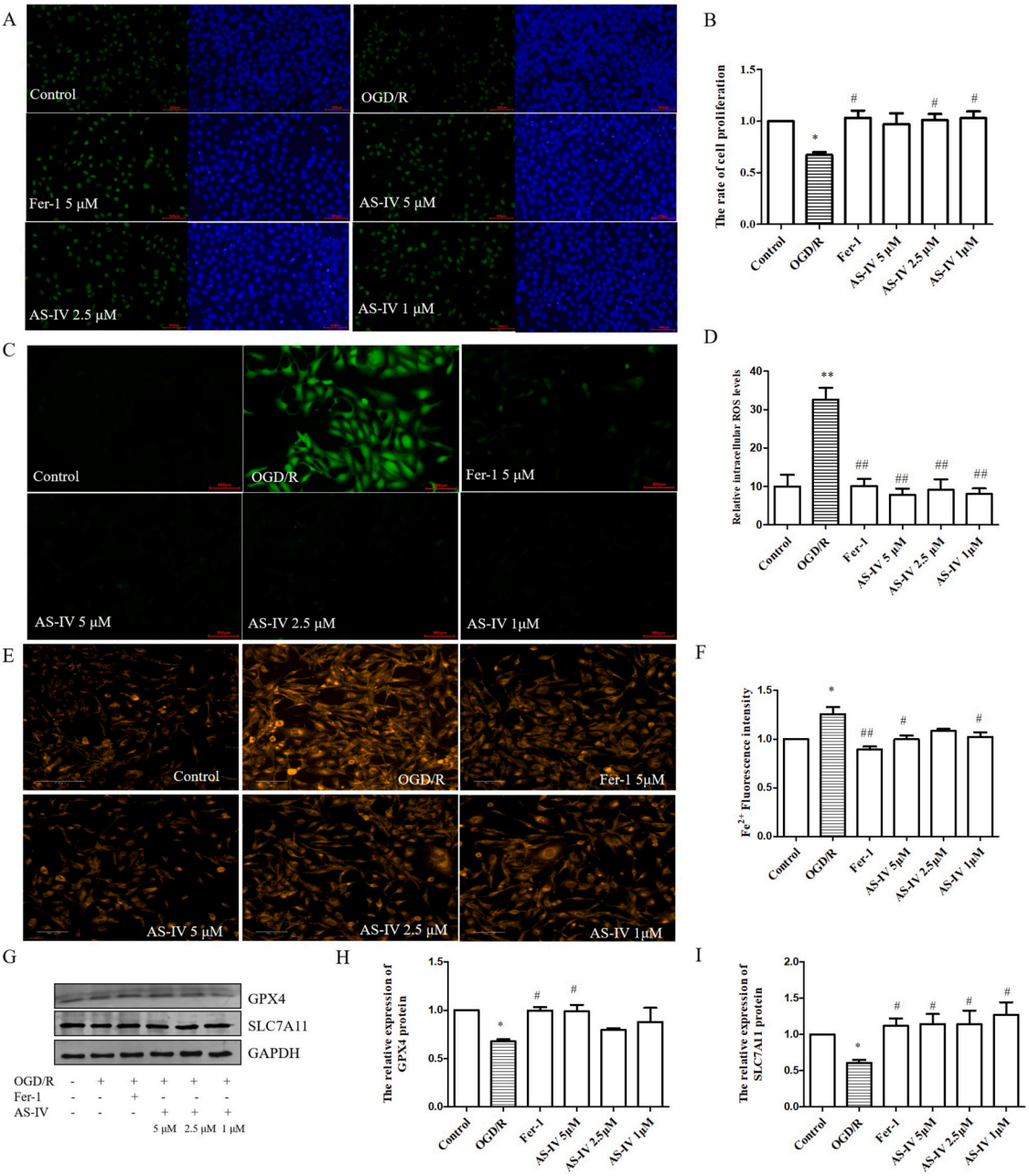

Fig. 6. AS-IV protected HUVECs against OGD/R injury as same as Fer-1. (A) Representative images of EdU staining. (B) Quantification of EdU staining. (C) Representative images of DCFH-DA staining. (D) Quantification of ROS level. (E) Representative images of FerroOrange staining. (F) Quantification of Fe^{2+} level. (G) Representative images of GPX4 and SLC7A11. (H–I)Quantitative data of GPX4 and SLC7A11 expressions. $^{*}P < 0.05$ vs. Control group; $^{\#}P < 0.05$ vs. OGD/R group.

4.7. Molecular dynamics (MD) simulation

A 100 ns MD simulation was performed to confirm the binding strengths between targets and AS-IV that were predicted by molecular docking using the GROMACS software package. Two protein-AS-IV complexes obtained by molecular docking were dissociated using PyMOL software. The topology of the protein was analyzed using charmm force field parameters, while the AS-IV were subjected to topology analysis by uploading it to the CGenFF server (https://cgenff.umaryland.edu/). The protein-ligand complex was created using the TIP3P water model with explicit solvent, and periodic boundary conditions were established by confining the system in a dodecahedral box. Chloride or sodium ions were added to balance the charge based on the deviation. The MD simulation workflow consists of four steps. First, the energy of the system was minimized using the steepest descent method with 50,000 steps, and the

minimization was stopped when the maximum force was <10.0 kJ/mol. Then, the complexes were categorized, proteins and ligands were grouped, and water and ions were grouped to achieve better temperature coupling. The systems were then kept in equilibrium at 300 K using the protein-ligand complex NVT equilibrium. Finally, a 100ns (100000 ps) MD simulation of the system was performed in the NPT combined mode. After the simulation, the protein was re-centered, and the protein skeleton was rotated and parallel-fitted to achieve smoother visualization later. The calculations and analyses of the simulation results led to the determination of the interaction energy, RMSD, RG, SASA files, which were visualized with the software QtGrace_v027.

4.8. HUVECs and treatments

4.8.1. Experiment groups and treatment

HUVECs were obtained from CellBio (Shanghai, China). The cells were divided into the following groups: (1) control group, (2) oxygen and glucose deprivation/reperfusion (OGD/R) group, (3) Fer-1 group, and (4)AS-IV group. All the cells cultured in MEM medium were exposed to hypoxia for 6 h in a chamber containing 94 % N_2, 5 % CO_2, and 1 % O_2 except for the control group. Afterwards, the cells were incubated for an additional 24 h in DMEM medium supplemented with Fer-1 and AS-IV under normoxic conditions for the Fer-1 and AS-IV groups.

4.8.2. Detection of cell proliferation

Cell proliferation was mesaured using a 5-Ethynyl-2′-deoxyuridine (EdU) assay (Beyotime) according to the manufacturer's protocol. Images were collected and analyzed in three randomly selected fields under a fluorescence microscope.

4.8.3. Measurement of ROS

A fluorescent probe sensitive to peroxide (DCFH-DA) was employed to determine the level of ROS. Briefly, HUVECs were incubated with 10 μM DCFH-DA for 30 min followed by washed twice with PBS. The fluorescence level of DCFH-DA detected by fluorescent microscopy, reflected the level of ROS.

4.8.4. Measurement of intracellular Fe^{2+} content

FerroOrange, a novel fluorescent probe, was used for the level of Fe^{2+} inside living cells. Briefly, HUVECs were incubated with 1 μM FerroOrange Working Solution for 30 min. The fluorescence intensity of FerroOrange detected by High Content Analysis System (PerkinElmer Operetta CLS) reflected the level of Fe^{2+}.

4.8.5. Western blot

HUVECs was lysed using 1× SDS sample buffer after washing with PBS twice. Subsequently, the lysates were heated at 95 °C for 10 min and then centrifuged at 12,000 rpm for 10 min. Total proteins were separated by SDS-PAGE and transferred onto PVDF membranes. Next, the membranes were incubated overnight at 4 °C with antibodies specific to GPX4 (1:1000), SLC7A11 (1:1000) and GPADH (1:10000). Afterwards, the membranes were washed and incubated with either IRDye 680RD Goat anti-Rabbit IgG (1: 20000) or Dylight 680 Goat anti-Mouse IgG (1: 20000) for fluorescent assays using LI-COR® Odyssey CLX equipment. Finally, the images were analyzed with the ImageJ software.

4.9. Statistical analysis

Statistical analysis was conducted using the GraphPad Prism 5 and data were presented as the mean ± SEM. One-way ANOVA followed by Tukey multiple comparison test was used to establish statistical significance. $P < 0.05$ was considered statistically significant.

Funding

This work was supported by the National Natural Science Foundation of China (grant numbers 81973560 and 82304763) and the Key Discipline Nephrology of Hangzhou (Integrated Traditional and Western Medicine) (grant numbers 2020SJZDXK01).

Author contributions

RCY and HTW conceived and designed the experiments. RCY, HTW and YG contributed reagents and materials. YG and JFW performed the experiments and wrote the paper. YJH, MYJ and WYX analyzed and interpreted the data. YPS, JHY revised the manuscript. All authors read and approved the final manuscript.

Data availability statement

The data are available from the corresponding author on reasonable request.

Declaration of competing interest

No conflict of interest exits in the submission of this manuscript, and manuscript is approved by all authors for publication.

References

[1] K. Lee, H.R. Jang, Role of T cells in ischemic acute kidney injury and repair, Korean J Intern Med 37 (3) (2022) 534–550, 10.3904/kjim.2021.526.
[2] P. Malko, L.H. Jiang, TRPM2 channel-mediated cell death: an important mechanism linking oxidative stress-inducing pathological factors to associated pathological conditions, Redox Biol. 37 (2020), 101755, 10.1016/j.redox.2020.101755.
[3] J.V. Bonventre, A. Zuk, Ischemic acute renal failure: an inflammatory disease? Kidney Int. 66 (2) (2004) 480–485, 10.1111/j.1523-1755.2004.761_2.x.
[4] P. Devarajan, Update on mechanisms of ischemic acute kidney injury, J. Am. Soc. Nephrol. 17 (6) (2006) 1503–1520, https://doi.org/10.1681/ASN.2006010017.
[5] D.Q. Zhang, J.S. Li, Y.M. Zhang, F. Gao, R.Z. Dai, Astragaloside IV inhibits Angiotensin II-stimulated proliferation of rat vascular smooth muscle cells via the regulation of CDK2 activity, Life Sci. 200 (2018) 105–109.
[6] L. Li, X. Hou, R. Xu, C. Liu, M. Tu, Research review on the pharmacological effects of astragaloside IV, Fundam. Clin. Pharmacol. 31 (1) (2017) 17–36, https://doi.org/10.1111/fcp.12232.
[7] L. You, Z. Fang, G. Shen, Q. Wang, Y. He, S. Ye, L. Wang, M. Hu, Y. Lin, M. Liu, A. Jiang, Astragaloside IV prevents high glucose-induced cell apoptosis and inflammatory reactions through inhibition of the JNK pathway in human umbilical vein endothelial cells, Mol. Med. Rep. 19 (3) (2019) 1603–1612, https://doi.org/10.3892/mmr.2019.9812.
[8] L. Tang, M. Zhu, X. Che, X. Yang, Y. Xu, Q. Ma, M. Zhang, Z. Ni, X. Shao, S. Mou, Astragaloside IV targets macrophages to alleviate renal ischemia-reperfusion injury via the crosstalk between hif-1α and NF-κB (p65)/Smad7 pathways, J. Personalized Med. 13 (1) (2022) 59, https://doi.org/10.3390/jpm13010059.
[9] B. Boezio, K. Audouze, P. Ducrot, O. Taboureau, Network-based approaches in pharmacology, Mol Inform 36 (10) (2017), 201700048, https://doi.org/10.1002/minf.201700048.
[10] Y. Xiong, Y. Yang, W. Xiong, Y. Yao, H. Wu, M. Zhang, Network pharmacology-based research on the active component and mechanism of the antihepatoma effect of Rubia cordifolia L, J. Cell. Biochem. 120 (8) (2019) 12461–12472, https://doi.org/10.1002/jcb.28513.
[11] A.L. Hopkins, Network pharmacology: the next paradigm in drug discovery, Nat. Chem. Biol. 4 (11) (2008) 682–690, https://doi.org/10.1038/nchembio.118.
[12] H. Zhang, S. Zhang, M. Hu, Y. Chen, W. Wang, K. Zhang, H. Kuang, Q. Wang, An integrative metabolomics and network pharmacology method for exploring the effect and mechanism of Radix Bupleuri and Radix Paeoniae Alba on anti-depression, J. Pharm. Biomed. Anal. 189 (2020), 113435, https://doi.org/10.1016/j.jpba.2020.113435.
[13] Y. Zheng, R. Li, Y. Zhou, S. Zhang, X. Fan, Investigation on the potential targets of Astragaloside IV against intracerebral hemorrhage based on network pharmacology and experimental validation, Bioorg. Chem. 127 (2022), 105975, https://doi.org/10.1016/j.bioorg.2022.105975.
[14] L.F. Luo, P. Guan, L.Y. Qin, J.X. Wang, N. Wang, E.S. Ji, Astragaloside IV inhibits adriamycin-induced cardiac ferroptosis by enhancing Nrf2 signaling, Mol. Cell. Biochem. 476 (7) (2021) 2603–2611, https://doi.org/10.1007/s11010-021-04112-6.
[15] X. Wang, Y. Wang, D. Huang, S. Shi, C. Pei, Y. Wu, Z. Shen, F. Wang, Z. Wang, Astragaloside IV regulates the ferroptosis signaling pathway via the Nrf2/SLC7A11/GPX4 axis to inhibit PM2.5-mediated lung injury in mice, Int. Immunopharm. 112 (2022), 109186, https://doi.org/10.1016/j.intimp.2022.109186.
[16] Z. Liu, Z. Zhou, P. Ai, C. Zhang, J. Chen, Y. Wang, Astragaloside IV attenuates ferroptosis after subarachnoid hemorrhage via Nrf2/HO-1 signaling pathway, Front. Pharmacol. 13 (2022), 924826, https://doi.org/10.3389/fphar.2022.924826.
[17] L.Y. Qin, P. Guan, J.X. Wang, Y. Chen, Y.S. Zhao, S.C. Yang, Y.J. Guo, N. Wang, E.S. Ji, Therapeutic potential of astragaloside IV against adriamycin-induced renal damage in rats via ferroptosis, Front. Pharmacol. 18 (13) (2022), 812594, https://doi.org/10.3389/fphar.2022.812594.
[18] X. Tang, X. Li, D. Zhang, W. Han, Astragaloside-IV alleviates high glucose-induced ferroptosis in retinal pigment epithelial cells by disrupting the expression of miR-138-5p/Sirt1/Nrf2, Bioengineered 13 (4) (2022) 8240–8254, https://doi.org/10.1080/21655979.2022.2049471.
[19] Y. Zhou, L. Li, C. Mao, D. Zhou, Astragaloside IV ameliorates spinal cord injury through controlling ferroptosis in H_2O_2-damaged PC12 cells in vitro, Ann. Transl. Med. 10 (21) (2022) 1176, https://doi.org/10.21037/atm-22-5196.
[20] S. Sheng, J. Xu, Q. Liang, L. Hong, L. Zhang, Astragaloside IV inhibits bleomycin-induced ferroptosis in human umbilical vein endothelial cells by mediating LPC, Oxid. Med. Cell. Longev. 2021 (2021), 6241242, https://doi.org/10.1155/2021/6241242.
[21] Q. He, C. Liu, X. Wang, K. Rong, M. Zhu, L. Duan, P. Zheng, Y. Mi, Exploring the mechanism of curcumin in the treatment of colon cancer based on network pharmacology and molecular docking, Front. Pharmacol. 14 (2023), 1102581, https://doi.org/10.3389/fphar.2023.1102581.
[22] Y. Wang, Y. Yuan, W. Wang, Y. He, H. Zhong, X. Zhou, Y. Chen, X.J. Cai, L.Q. Liu, Mechanisms underlying the therapeutic effects of Qingfeiyin in treating acute lung injury based on GEO datasets, network pharmacology and molecular docking, Comput. Biol. Med. 145 (2022), 105454, https://doi.org/10.1016/j.compbiomed.2022.105454.
[23] E. Mukherjee, K. Pfister, Y.L. Phua, K. Shaikh, B.T. Sanders, S.L. Hemker, P.J. Pagano, Y.L. Wu, J. Ho, S. Sims-Lucas, Endothelial-derived miR-17∼92 promotes angiogenesis to protect against renal ischemia-reperfusion injury, J. Am. Soc. Nephrol. 32 (2021) 553–562, https://doi.org/10.1681/asn.2020050717.
[24] W.Q. Ma, X.J. Sun, Y. Zhu, N.F. Liu, Metformin attenuates hyperlipidaemia-associated vascular calcification through anti-ferroptotic effects, Free Radic. Biol. Med. 165 (2021) 229–242, https://doi.org/10.1016/j.freeradbiomed.2021.01.033.
[25] E. Park, S.W. Chung, ROS-mediated autophagy increases intracellular iron levels and ferroptosis by ferritin and transferrin receptor regulation, Cell Death Dis. 10 (11) (2019) 822, https://doi.org/10.1038/s41419-019-2064-5.
[26] B.R. Stockwell, J.P.A. Friedmann, H. Bayir, A.I. Bush, M. Conrad, S.J. Dixon, S. Fulda, S. Gascón, S.K. Hatzios, V.E. Kagan, K. Noel, X. Jiang, A. Linkermann, M. E. Murphy, M. Overholtzer, A. Oyagi, G.C. Pagnussat, J. Park, Q. Ran, C.S. Rosenfeld, D.D. Zhang, Ferroptosis: a regulated cell death Nexus linking metabolism, redox biology, and disease, Cell 171 (2) (2017) 273–285, https://doi.org/10.1016/j.cell.2017.09.021.
[27] Y. Xie, W. Hou, X. Song, Y. Yu, J. Huang, X. Sun, R. Kang, D. Tang, Ferroptosis: process and function, Cell Death Differ. 23 (3) (2016) 369–379, https://doi.org/10.1038/cdd.2015.158.
[28] J.Y. Cao, S.J. Dixon, Mechanisms of ferroptosis, Cell. Mol. Life Sci. 73 (11–12) (2016) 2195–2209, https://doi.org/10.1007/s00018-016-2194-1.
[29] P. Lei, T. Bai, Y. Sun, Mechanisms of Ferroptosis and relations with regulated cell death: a review, Front. Physiol. 10 (2019) 139, https://doi.org/10.3389/fphys.2019.00139.
[30] X. Song, S. Zhu, P. Chen, W. Hou, Q. Wen, J. Liu, Y. Xie, J. Liu, D.J. Klionsky, G. Kroemer, M.T. Lotze, H.J. Zeh, R. Kang, D. Tang, AMPK-mediated BECN1 phosphorylation promotes ferroptosis by directly blocking system xc-activity, Curr. Biol. 28 (15) (2018) 2388–2399, https://doi.org/10.1016/j.cub.2018.05.094, e5.
[31] P. Liu, Y. Feng, H. Li, X. Chen, G. Wang, S. Xu, Y. Li, L. Zhao, Ferrostatin-1 alleviates lipopolysaccharide-induced acute lung injury via inhibiting ferroptosis, Cell. Mol. Biol. Lett. 25 (2020) 10, https://doi.org/10.1186/s11658-020-00205-0.
[32] D.H. Kim, W.D. Kim, S.K. Kim, D.H. Moon, S.J. Lee, TGF-β1-mediated repression of SLC7A11 drives vulnerability to GPX4 inhibition in hepatocellular carcinoma cells, Cell Death Dis. 11 (5) (2020) 406, https://doi.org/10.1038/s41419-020-2618-6.
[33] K. Bersuker, J.M. Hendricks, Z. Li, L. Magtanong, B. Ford, P.H. Tang, M.A. Roberts, B. Tong, T.J. Maimone, R. Zoncu, M.C. Bassik, D.K. Nomura, S.J. Dixon, J. A. Olzmann, The CoQ oxidoreductase FSP1 acts parallel to GPX4 to inhibit ferroptosis, Nature 575 (7784) (2019) 688–692, https://doi.org/10.1038/s41586-019-1705-2.